Cancer Letters 447 (2019) 75–85

Contents lists available at ScienceDirect

Cancer Letters

journal homepage: www.elsevier.com/locate/canlet

Original Articles

Novel half-sandwich iridium O^C (carbene)-Complexes: *In vitro* and *in vivo* tumor growth suppression and pro-apoptosis via ROS-mediated cross-talk between mitochondria and lysosomes

Zhishan Xu[a,b], Yujiao Zhang[b], Shumiao Zhang[b], Xianglei Jia[c], Genshen Zhong[d], Yuliang Yang[b], Qing Du[b], Juanjuan Li[b], Zhe Liu[b,*]

[a] College of Chemistry, Chemistry Engineering and Materials Science, Shandong Normal University, Jinan, 250014, China
[b] Institute of Anticancer Agents Development and Theranostic Application, The Key Laboratory of Life-Organic Analysis and Key Laboratory of Pharmaceutical Intermediates and Analysis of Natural Medicine, Department of Chemistry and Chemical Engineering, Qufu Normal University, Qufu, 273165, China
[c] Henan Key Laboratory of Neural Regeneration, The First Affiliated Hospital of Xinxiang Medical University, Weihui, 453100, China
[d] Henan Collaborative Innovation Center of Molecular Diagnosis and Laboratory Medicine, School of Laboratory Medicine, Xinxiang Medical University, Xinxiang, 453003, China

ARTICLE INFO

Keywords:
Half-sandwich Ir—NHC complexes
Tumor growth inhibition
ROS
Mitochondrial damage
Lysosomal disruption

ABSTRACT

Herein we present half-sandwich Ir^{III} complexes [(η^5-Cp^{xbiph})Ir(O^C)Cl] containing O^C(NHC)-chelating ligand as anticancer and antimetastasis agents. All the complexes displayed high potency *in vitro* against a wide range of cancer cells. In addition, Ir2 significantly curb tumor growth in a colon cancer mouse xenograft model *in vivo*. Further mechanism of action studies indicate that Ir2-initiated apoptosis occurs through ROS-mediated cross-talk between mitochondria and lysosomes.

1. Introduction

Cancer has become one of the most urgent health care challenges that modern medicine faces today in which cancer metastasis and resistance phenomena are the two main intractable problems of cancer therapy in the clinic [1–3]. Tremendous efforts have been devoted to develop more effective anticancer drugs and therapeutic strategies, yet rapid drug resistance development of the cancerous tissues means that only a few chemotherapy agents have been registered to date [4].

Few metal-based chemotherapy agents are available, but play key roles in clinical chemotherapy, such as cisplatin and its derivatives [5]. However, there is a pressing need to replace the extensively employed platinum compounds because of drug resistance and nephrotoxicity which limit their clinical practice [6]. In addition, ruthenium (Ru)-based complexes have also attracted significant attention due to their good biochemical properties [7–12]. Moreover, Iridium (Ir)-based complexes have emerged as promising therapeutic agents to non-platinum metal-based anticancer compounds because of their multiple anticancer mechanism of action (MoA) [13–22]. Our group also has reported recently a series of Ru and Ir-based complexes which demonstrated significant anticancer activity [23–29].

N-Heterocyclic carbene (NHC) is a cyclic neutral ligand with outstanding σ donor and poor π acceptor abilities, in that it forms stable transition complexes with most transition metals and are now widely applied in catalysis and metallodrug development nowadays [30–33]. In recent years, Ir—NHC complexes have been used for numerous applications in the field of catalysis but investigations as potential therapeutic agents are also in progress [34]. Half-sandwich Ir complexes containing NHC have also been successfully employed as potential catalysts for a variety of reactions [35]. Recently, we reported half-sandwich Ir—NHC complexes bearing C^C-chelating ligands with potent anticancer activity against cancer cells [36]. Although half-sandwich Ir—NHC complexes display promising anticancer activity, till now, little information of half-sandwich Ir^{III} complexes containing O^C(NHC)-chelating ligand as anticancer agents is available, in particular, tumor growth suppression *in vivo* and MoA remain uncertain. Hence, we choose O^C(NHC)-chelating ligand with hard anionic building blocks because of its excellent stability for Ir^{III}. The anionic group could increase the stability by enhancing the bond between the NHCs and the metal center. Herein four half-sandwich Ir—NHC complexes [(η^5-Cp^{xbiph})Ir(O^C)Cl] were synthesized, Scheme 1A. Furthermore, the MoA of anticancer was investigated in A549 cancer cells. Finally, the antitumor effect of Ir2 was assessed in a CT26 colon cancer mouse xenograft model and it was the first report of half-sandwich Ir compound

* Corresponding author.
E-mail address: liuzheqd@163.com (Z. Liu).

https://doi.org/10.1016/j.canlet.2019.01.018
Received 9 October 2018; Received in revised form 8 January 2019; Accepted 17 January 2019

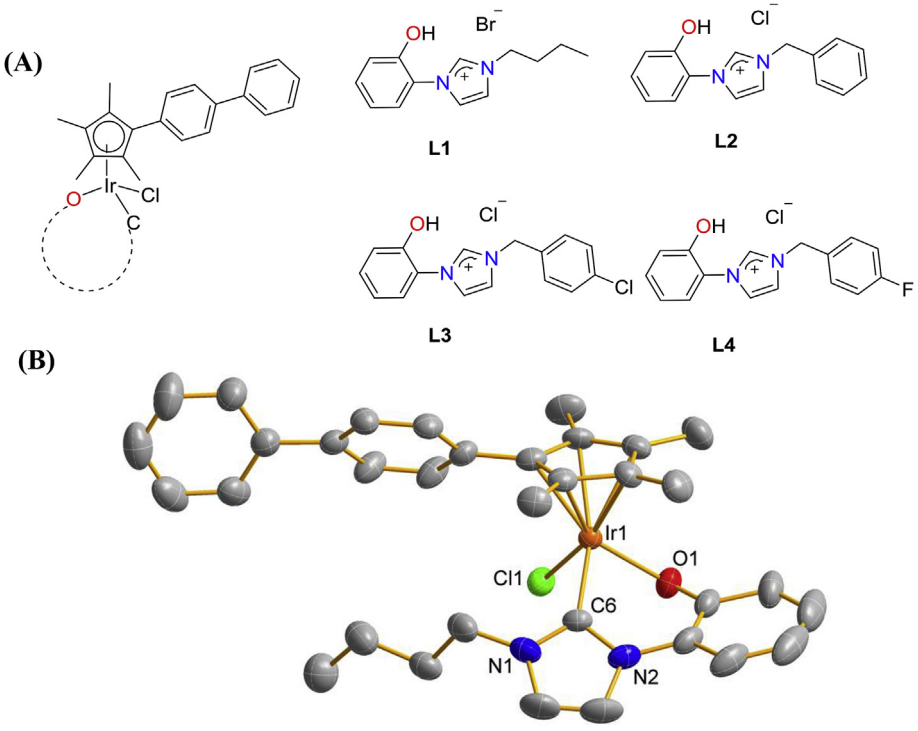

Scheme 1. (A) Chemical structures of studied complexes Ir1−Ir4. (B) X-ray crystal structure of complex Ir1.

that inhibits tumor growth *in vivo*. Our work may provide new cancer therapeutic potential for metal-based anticancer agents.

2. Materials and methods

2.1. Materials

$IrCl_3 \cdot nH_2O$, Ag_2O, 1H-imidazole, 2-bromoanisole, n-butyl bromide, benzyl chloride, 4-fluoro-1-(chloromethyl)-benzene and 1-chloro-4-(chloromethyl)-benzene were purchased from Sigma-Aldrich.

2.2. Cells and reagents

BEAS-2B, 16HBE, HeLa cells, A549 cells, HT29 cells, HCT116 cells, GL261 cells, HepG2 cells and CT26 cells were preserved by our laboratory and were grown in Dubelco's Modified Eagle Medium (DMEM) supplemented with 10% fetal bovine serum and 1% (v/v) penicillin-streptomycin solution. All cells were grown at 37 °C in a humidified incubator under a 5% CO_2 atmosphere. MTT and phosphate-buffered saline (PBS) were purchased from Sangon Biotech. Hoechst 33342 and Magic Red MR-$(RR)_2$ was purchased from Immunochemistry Tech. Bcl-2 rabbit polyclonal antibody, Bax rabbit polyclonal antibody, LAMP1 rabbit polyclonal antibody and FITC-conjugated goat anti-rabbit IgG were purchased from Proteintech. IFN-γ was purchased from Pepro Tech. Phycoerythrin (PE) anti-PD-L1 was purchased from BioLegend. CA-074 Me was purchased from ApexBio.

2.3. Cell viability

BEAS-2B, 16HBE, HeLa cells, A549 cells, HT29 cells, HCT116 cells, GL261 cells, HepG2 cells and CT26 cells (5000 cells/96-well plates) were preincubated in drug-free media overnight before adding different concentrations of the compounds to be tested. The stock solution of the solid complexes Ir1−Ir4, L1-L4 and dimer were dissolved in DMSO. After exposure to different concentrations of complexes Ir1−Ir4 and L1-L4 for 24 h, cell viability were measured by using the MTT assay and using a microplate reader (DNM-9606, Perlong Medical, Beijing, China) at an absorbance of 570 nm. IC_{50} values quoted are mean ± standard deviation.

2.4. Cellular uptake assay

A549 cells (5×10^6/10 ml per dish) were seeded in 100 mm dishes overnight, then media was replaced with fresh media containing the tested complexes Ir1−Ir4 at concentration 5 μM for 12 h. The cells were collected and counted using the automated cell counter and were digested with concentrated nitric acid (65%, 50 μl) at 95 °C for 0.5 h, then further adding 100 μl H_2O_2 at 95 °C for 1 h, subsequently 75 μl concentrated HCl was added at 95 °C for 0.5 h. The solution was then diluted to a final volume of 1 ml with Milli-Q water. The concentration of Ir was determined by ICP-MS.

2.5. Wound healing assay

Wound healing assay was performed using A549 cancer cells. Briefly, A549 cells were plated into 6-well plates at a density of 5.0×10^5 cells per well and allowed to grow for 24 h. Then the monolayer cells were wounded by scratching with 20 μl pipette tips and unattached cells were washed with PBS. Fresh medium with 1% FBS was used to suppress cell proliferation, then containing the concentrations of 0.125 × IC_{50}, 0.25 × IC_{50}, and 0.5 × IC_{50} of complex Ir2 were added to plates. At specific time intervals (0 h and 24 h), images were taken. The wound width was measured in order to evaluate the wound healing ability of tested cells.

2.6. Transwell migration assay

Transwell migration assays were performed by using transwell chamber in 24-well cell culture plate with 8 μm pores. Chambers were washed with PBS for three times. Then the 600 μl medium with the tested compounds at concentration of IC_{50} was placed in the lower chamber, and A549 cancer cells (2×10^5/well) in 200 μl serum-free medium were seeded in the top chamber. Cells were treated with containing the concentrations of 0.125 × IC_{50}, 0.25 × IC_{50}, and

0.5 × IC_{50} of complexes Ir2 at 37 °C in a humidified atmosphere of 5% CO_2. After incubation for 24 h, non-migrated cells on the top surface of the membrane were gently scraped away with cotton swab, and migrated cells were fixed with 4% paraformaldehyde for 20 min and stained with 0.1% crystal violet for 30 min. The cells that migrated to the lower side of the membranes were imaged and counted using a microscope.

2.7. Colony formation assay

After plating 1000 of A549 cancer cells per well in 12-well plates, cells treated with containing the concentrations of 0.125 × IC_{50}, 0.25 × IC_{50}, and 0.5 × IC_{50} of complexes Ir2 were cultured for 10 days for the development of macroscopic colonies and the medium was changed every 3 days. The plates were washed three times with PBS and fixed with 4% paraformaldehyde for 20 min. All cells were stained with 0.1% crystal violet, then washed with distilled water to remove excess stain.

2.8. GILA assays

The GILA (growth in low attachment) assay was used to assess the growth of A549 cells. Briefly, A549 cells at 5.0 × 10^3 per well were seeded in a ultra-low attachment 6-well, cells treated with containing the concentrations of 0.125 × IC_{50}, 0.25 × IC_{50}, and 0.5 × IC_{50} of complexes Ir2 were cultured for 10 days for the development of sphere formation. The sphere formation were imaged with a microscope.

2.9. Cell cycle distribution

A549 cells were harvested using trypsin-EDTA and fixed for 24 h in cold 70% ethanol. DNA was stained in PBS containing propidium iodide (PI) and RNase. Cell pellets were washed and resuspended in PBS before being analyzed by a flow cytometer (ACEA NovoCyte, Hangzhou, China). Data were processed using NovoExpress™ software.

2.10. Induction of apoptosis

Flow cytometry analysis of apoptotic populations of the cells caused by exposure to complex Ir2 was carried out using the Annexin V-PE/7-AAD apoptosis Detection Kit (KeyGEN BioTECH, China) according to the supplier's instructions. The samples were analyzed by a flow cytometer (ACEA NovoCyte, Hangzhou, China). Apoptosis was also confirmed by fluorescence microscopy after staining with Hoechst 33342. The cells were washed with PBS twice and visualized by confocal microscopy (LSM 880 NLO, Carl Zeiss, Germany). Emission was collected at 450 ± 20 nm upon excitation at 405 nm.

2.11. Mitochondrial membrane potential assay

A549 cancer cells (1.0 × 10^6 per well) were seeded in six-well and incubated with 0.5 × IC_{50}, 1 × IC_{50} and 2 × IC_{50} of complex Ir2 for 24 h. For positive controls, the cells were exposed to carbonyl cyanide 3-chlorophenylhydrazone, CCCP (5 μM) for 20 min. Analysis of the changes of mitochondrial potential in cells was carried out using the mitochondrial membrane potential assay kit with JC-1 according to the manufacturer protocol (Beyotime Institute of Biotechnology, Shanghai, China). All samples were analyzed using a flow cytometer (ACEA NovoCyte, Hangzhou, China). Data were processed using NovoExpress™ software.

2.12. ROS determination assay

A549 cancer cells (1.0 × 10^6 per well) were seeded in six-well and incubated with 0.5 × IC_{50}, 1 × IC_{50} and 2 × IC_{50} of complex Ir2 for 24 h cells, and then incubated with the DCFH-DA probe (10 μM) at 37 °C for 30 min. ROS generation caused by exposure to complex Ir2 was carried out using the Reactive Oxygen Species Assay Kit according to the manufacturer protocol (Beyotime Institute of Biotechnology, Shanghai, China). The fluorescence intensity was analyzed by flow cytometry (ACEA NovoCyte, Hangzhou, China).

2.13. Flow cytometry analysis for caspase 3, PARP, Bax, Bcl-2, LAMP1 and PD-L1

A549 cancer cells (1.0 × 10^6/2 ml per well) were seeded in a six-well plate. For inhibition studies, cells were pre-treated with NAC (10 mM) for 1 h followed by incubation with the tested complex Ir2 at the 1 × IC_{50} concentration for 24 h. Then the cells were harvested and stained with specific antibody of cleaved Caspase-3, PARP, Bax, Bcl-2, LAMP1 and PD-L1 according to the manufacturer's instructions and analyzed by flow cytometry (ACEA NovoCyte, Hangzhou, China). Data were analyzed using by NovoExpress™ software.

2.14. Antitumor evaluation of Ir2 in xenograft tumor animal models

The mouse CT26 animal experiments were performed with 7-week-old female BALB/c mice (20–23 g). Animal care, experiments, and killing were performed following the principles stated in the Guide for the Care and Use of Laboratory Animals. All efforts were made to minimize animal suffering during the experiments. The mice were acclimated for 7 days after arrival before experiments started. For the establishment of tumor models in mice, CT26 cells suspended in saline were inoculated subcutaneously (Day 0) at the right axilla of the mouse with 1.0 × 10^6 cells/0.1 ml/mouse. At day 3, the mice were randomized into treatment groups (n = 6 per group). Then the treatments were started (intravenously injection twice at day 3 after tumor implantation), mice were injected in the tail vein with Ir2 (3 mg/kg and 5 mg/kg), respectively. Control mice were injected with saline. Tumor growth was measured with a caliper, and tumor volumes were calculated. The experiment was terminated at day 24, and the tumors were excised, weighed and imaged. The tumor volume was calculated by formula $V = ab^2 \times 0.52$, where a and b were the longest and shortest diameters of the tumor separately. The mean tumor weight was calculated and the results were expressed as the mean ± standard deviation.

2.15. Statistical analysis

Results are expressed as means ± standard deviations and significance was performed using ANOVA and the Student's t-test (*$p < 0.05$, **$p < 0.01$).

3. Results and discussion

3.1. Synthesis and characterization

The NHC ligands L1-L4 and the half-sandwich complexes Ir1−Ir4 were prepared by revised literature methods [37,38]. In general, the respective ligand and Ag_2O in CH_2Cl_2 were stirred for 2 h at room temperature, then K_2CO_3 and dimer $[(\eta^5\text{-}Cp^{xbiph})IrCl_2]_2$ were added to the mixture and reacted for 4 h to give complexes Ir1−Ir4. Complexes Ir1−Ir4 were characterized by ^{1}H NMR spectroscopy (Figs. S1–4, ESI†), ^{13}C NMR (Figs. S5–8, ESI†), ESI-MS (Figs. S9–12, ESI†), and elemental analysis. Crystal of complex Ir1 suitable for X-ray crystallography was obtained by slow diffusion of n-hexane into the concentrated dichloromethane solutions. Perspective view of the crystal structure of complex Ir1 is shown in Scheme 1B. Crystallographic and structural refinement data of Ir1 are summarized (Tables S1–2, ESI†). The crystal of Ir1 exhibited half-sandwich pseudo-octahedral, which proved the coordination of NHC and phenate groups with the iridium center. The Ir-$C_{carbene}$ and Ir−O (chelating ligand) distances are 2.023 Å and

Table 1
IC_{50} values (μM) of Ir^{III} complexes, L1-L4 and dimer against cancerous and normal cell lines.

Complex	A549	CT26	GL261	HCT116	HeLa	HepG2	HT29	16HBE	BEAS-2B
Ir1	5.0 ± 0.6	5.4 ± 0.8	9.1 ± 1.5	6.8 ± 0.3	4.7 ± 0.2	5.7 ± 0.5	6.3 ± 0.9	6.9 ± 0.5	7.4 ± 0.8
Ir2	3.7 ± 0.5	4.0 ± 0.1	7.4 ± 0.7	5.2 ± 0.5	3.9 ± 0.7	4.3 ± 0.2	5.0 ± 0.5	5.4 ± 0.9	5.8 ± 0.2
Ir3	3.8 ± 0.2	4.3 ± 0.3	8.1 ± 0.4	5.1 ± 0.9	4.2 ± 0.5	4.7 ± 0.6	5.3 ± 0.3	6.3 ± 0.6	7.4 ± 0.8
Ir4	4.0 ± 0.7	4.6 ± 0.5	7.7 ± 0.6	5.9 ± 0.1	4.0 ± 0.8	4.4 ± 0.4	4.8 ± 0.7	6.5 ± 0.4	7.9 ± 0.7
L1	> 100	> 100	> 100	> 100	> 100	> 100	> 100	> 100	> 100
L2	> 100	> 100	> 100	> 100	> 100	> 100	> 100	> 100	> 100
L3	> 100	> 100	> 100	> 100	> 100	> 100	> 100	> 100	> 100
L4	> 100	> 100	> 100	> 100	> 100	> 100	> 100	> 100	> 100
Dimer	> 50	> 50	> 50	> 50	> 50	> 50	> 50	> 50	> 50
Cisplatin	21.3 ± 1.7	23.7 ± 2.1	42.9 ± 1.8	44.6 ± 2.4	7.8 ± 0.3	22.7 ± 1.1	17.5 ± 0.9	17.9 ± 1.5	38.4 ± 2.8

2.104 Å, respectively, and the Ir—Cl bond length is 2.4098 Å. The bond distances are close to those reported similar substances. The distance from the Ir center to the η^5-cyclopentadienyl centroid is 1.8147 Å.

3.2. Cytotoxicity

The antiproliferative activities of complexes Ir1—Ir4 were determined against a wide range of cancer cell lines by MTT assay after a 24 h treatment *in vitro*. The resulting IC_{50} values are listed in Table 1. Complexes Ir1—Ir4 displayed higher cytotoxicity than cisplatin against 7 cancer cell lines, in particular, complex Ir2 showed about an 8-fold higher potency than cisplatin in HCT116 cells. Although the IC_{50} values fell in a relatively narrow range (from 3.7 μM to 9.1 μM), the differences demonstrated that the replacement of the n-butyl on the imidazole ring by benzyl group led to slight effects on their antiproliferative activities in different cancer cell lines. However, further analysis showed no effect on the antiproliferative activities when halogens were introduced into the para-position on the benzyl groups compared to that of the benzyl group. Unfortunately, all the complexes Ir1—Ir4 were found to be cytotoxic toward human bronchial epithelial normal cells BEAS-2B and 16HBE, i. e. no selectivity was observed for cancer cells versus normal cells with these complexes. In addition, it should also be noted that ligands L1-L4 were inactive against all cells screened (IC_{50} > 100 μM), whilst dimer showed slight activity (IC_{50} > 50 μM). Very excitingly, the integration of dimer with ligands resulted in significant improvement in antiproliferative activity, indicating a strong synergistic effect.

3.3. Lipophilicity, cellular uptake and stability

It is well known that the cellular uptake levels of Ir and Ru-based complexes are affected by lots of factors, such as lipophilicity, molecular size, and water-solubility [39]. The partition coefficient in octanol/water (log $P_{o/w}$) provides a measure of drug lipophilicity, which implies the cell-penetrating abilities of complexes. The log $P_{o/w}$ values measured using ICP-MS for complexes Ir1—Ir4 were 0.32, 0.54, 0.56 and 0.53, respectively (Table S3, ESI†). Additionally, the cellular accumulation of metal-based complexes has a critical influence on its cytotoxic activity. Cellular accumulation of complexes Ir1—Ir4 after 12 h treatment with at equipotent (IC_{50}) concentrations inside the A549 cells was determined using ICP-MS. The cellular accumulation amounts for complexes Ir1—Ir4 are 52.7, 80.5, 76.2 and 79.1 (ppb/10^6 cells), respectively (Table S3, ESI†), most likely due to the replacement of the n-butyl on the imidazole ring by benzyl group which increases the lipophilicity of complexes, thereby enhancing the cell-penetrating abilities of these Ir complexes and thus lead to enhanced cytotoxicity. These results are consistent with reports that the lipophilicity is positively associated with cytotoxic activity for Ir-based anticancer complexes [40]. Finally, to evaluate the stability of complexes Ir in DMSO-d_6, studies were performed by ^{1}H NMR spectroscopy at 310 K for complex Ir2. The ^{1}H NMR experiment result indicated that complex Ir2 was stable in 60% DMSO-d_6/40% D_2O at 310 K over 7 days (Fig. 1).

3.4. Inhibition of cell migration

Malignant cells acquiring metastatic capabilities are able to migrate to distant organ sites and adapt to the new microenvironments and survive, and eventually induce angiogenesis [41,42]. We investigated the inhibition effect of Ir2 on A549 cells migration by wound healing assays and transwell migration assays. Upon wound healing assays, Ir2 (0.5 × IC_{50}) inhibited A549 cells migration at a wound closure ratio of 15.9% compared to control group of 74.8%. The wound healing of A549 cancer cells was markedly attenuated after 24 h treatment of Ir2 compared to the control group. To further verify the antimetastatic properties of the Ir2 complex, transwell assays were conducted. The migrated A549 cells were stained with crystal violet and recorded by microscopic observations after Ir2 treatment for 24 h. In comparison with the control group in which migrated cells are counted as 100%, Ir2 (0.25 × IC_{50} and 0.5 × IC_{50}) could decrease dramatically cells migration ratios to 45.7% and 17.3%, respectively (Fig. 2 and Fig. S13, ESI†). These results revealed that Ir2 could impede effectively A549 cells metastasis.

3.5. Inhibition of colony formation

As for metastatic colonization, metastatic cells survive at new sites and thereafter proliferate to form secondary tumors [43], firstly, we measured the inhibition of colony formation induced by Ir2 at different concentrations in A549 cells. As shown in Fig. 3A, colony formation was inhibited after treatment with Ir2 at the indicated concentrations for 10 days. In addition, sphere formation assays also were performed to measure the inhibition of cells sphere formation potential induced by Ir2 at different concentrations for 10 days. The results showed that the size of the spheroid of A549 cells treated with Ir2 gradually decreased with the increase in Ir2 concentrations with respect to the size of the spheroid of the control group (Fig. 3B).

3.6. Induction of cell cycle arrest

We investigated whether the observed anti-proliferation activity of complex Ir2 is due to induction of cell cycle arrest. After A549 cells were treated with complex Ir2 at the indicated concentrations for 24 h, the cell cycle distribution was determined by using flow cytometry. The percentage of cells at the G_2/M phase is 7.3% in the control group. However, treatment with complex Ir2 (0.5 × IC_{50} and 1 × IC_{50}) increased percentage of these cells at G_2/M phase to 16.1% and 19.4%, respectively (Fig. S14 and Tables S4–1, ESI†). Additionally, at a concentration of 2 × IC_{50}, the percentage of cells at the G_2/M phase increased to 27.9% as compared to the control (10.5%). Meanwhile, the percentage of G_0/G_1 phase was decreased in a concentration-dependent manner (Fig. S14 and Tables S4–2, ESI†). These results suggest that the anti-proliferation effect induced by complex Ir2 in A549 cells could occur in G_2/M phase.

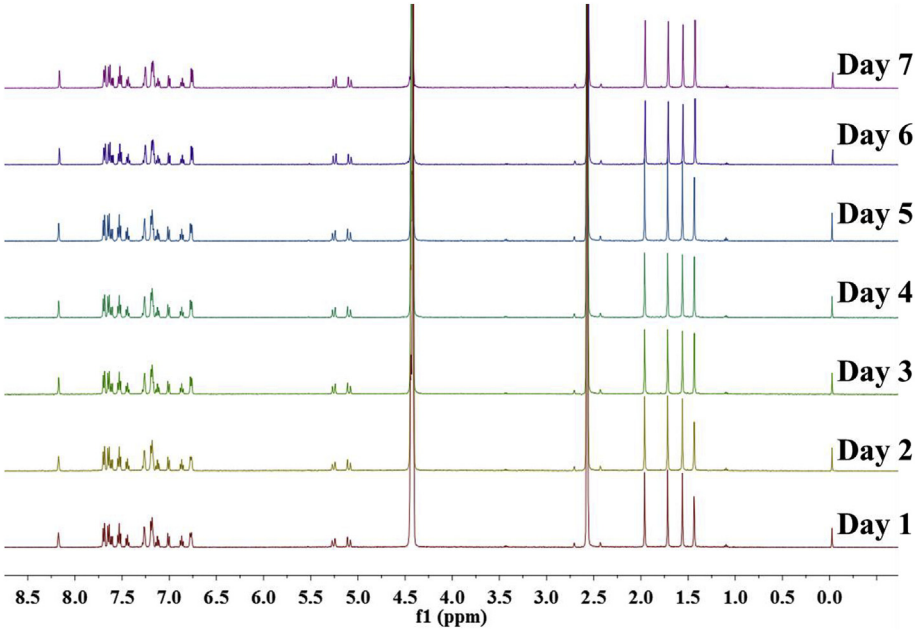

Fig. 1. The ^{1}H NMR spectra of the complex Ir2 at a concentration of 1.5 mM in 60% DMSO-d_6/40% D_2O at 310 K over 7 days.

3.7. Induction of apoptosis

Apoptosis is a common cell death pathway in metal-based drugs treatments [44]. To interrogate the observed reduction in cell viability caused by Ir2 is dependent on induction of apoptosis, an AnnexinV-PE/7-AAD double staining was performed and followed by flow cytometry analysis. A549 cells treated at the indicated concentrations showed Annexin V and 7-AAD positive populations. The apoptosis analysis showed a dose-dependent increase in the percentage of apoptosis. The percentage of apoptosis increased to 68.5% after A549 cells were treated with the 2 × IC_{50} concentration. As summarized in Fig. 4 and Table S5, ESI†. Obviously, these results suggest complex Ir2 could trigger an apoptotic response in A549 cells.

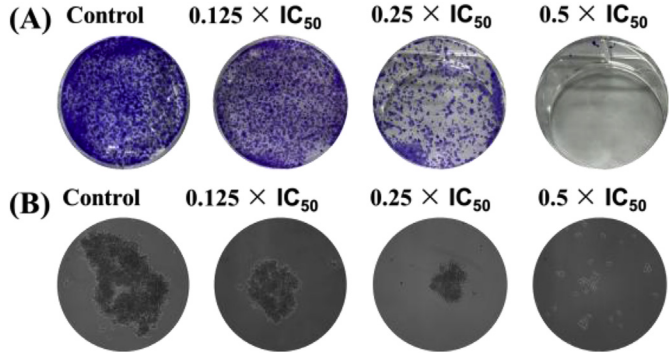

Fig. 3. A549 cells were incubated with Ir2 complexes for 10 days. Inhibition of colony formation (A) and sphere formation (B) induced by Ir2 for 10 days at the indicated concentrations.

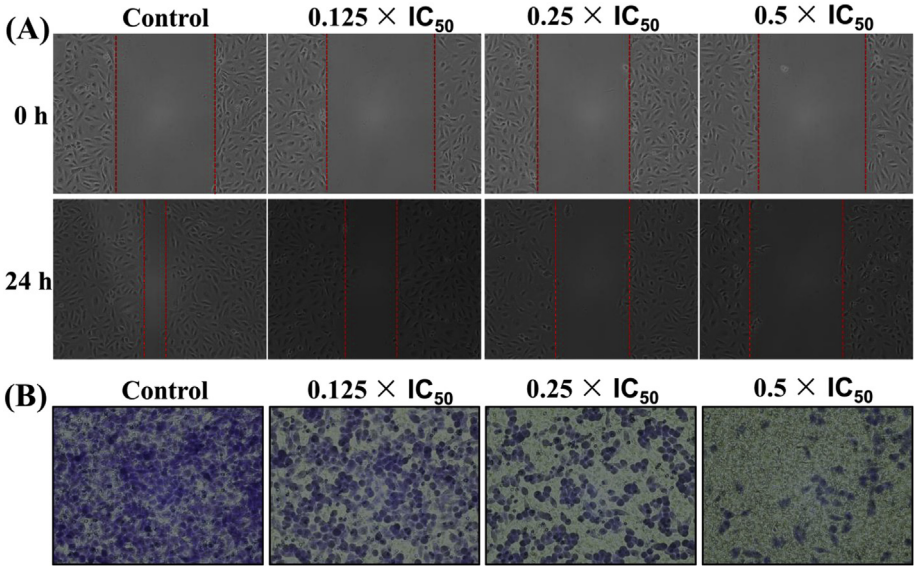

Fig. 2. A549 cells treated with complex Ir2 at indicated concentrations. For Wound-healing assay, typical images were taken at 0 and 24 h (A). For migration assay, typical images were taken at 24 h (B).

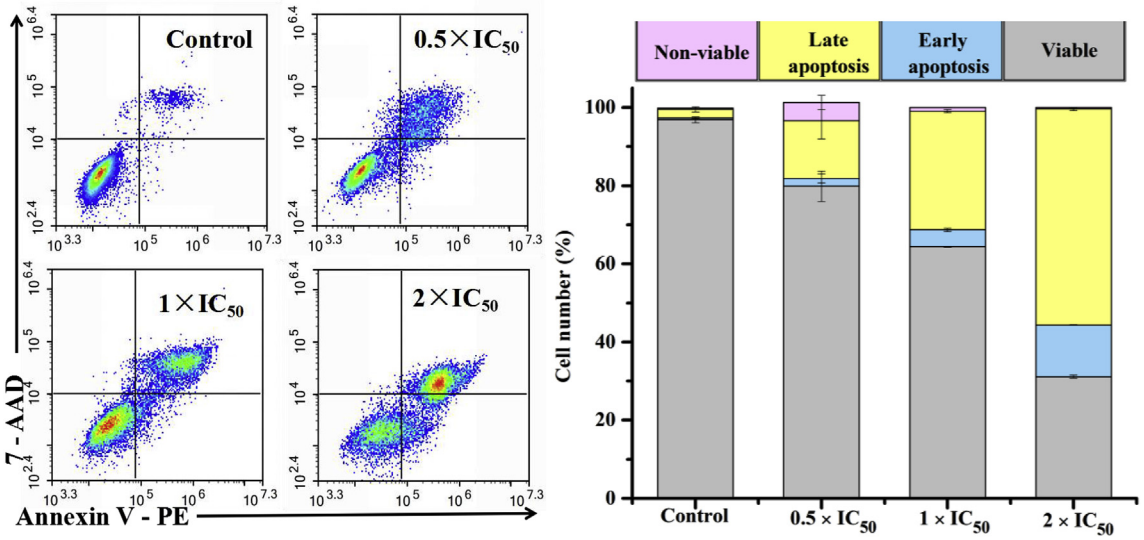

Fig. 4. Apoptosis analysis of A549 cells after 24 h of exposure to Ir2 was determined by flow cytometry using Annexin V-PE/7-AAD staining.

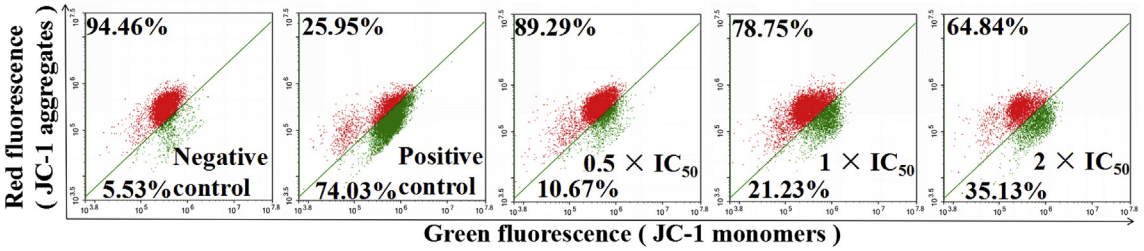

Fig. 5. Changes in mitochondrial membrane potential of A549 cancer cells induced by complexes Ir2 at concentrations of 0.5 × IC_{50}, 1 × IC_{50} and 2 × IC_{50}. Populations of cells that exhibit a reduction in the mitochondrial membrane potential.

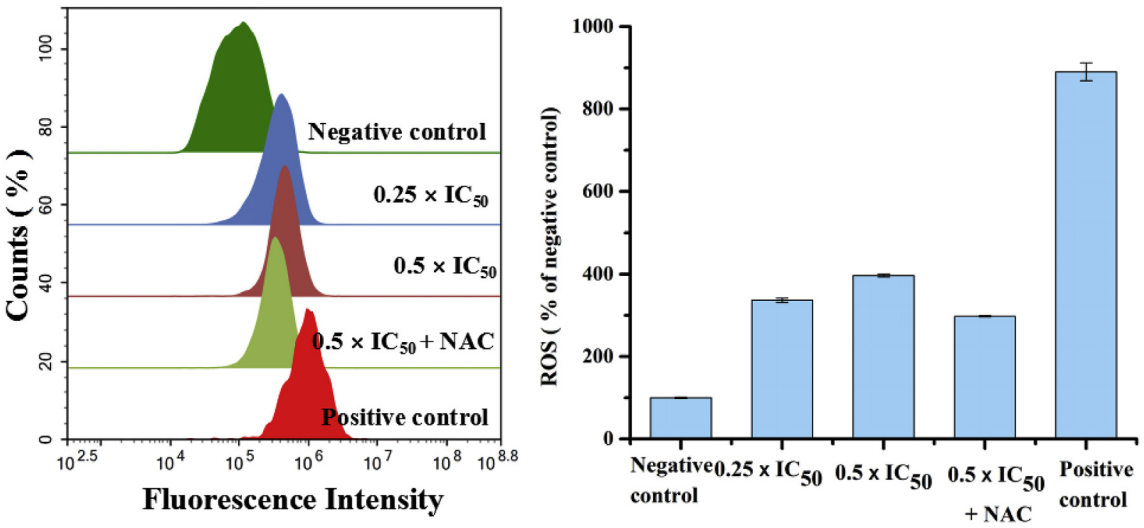

Fig. 6. Flow cytometric analysis of complex Ir2 induced ROS generation. A549 cells stained with DCFH-DA after treatment by indicated concentrations of complex Ir2 for 24 h. For inhibition studies, cells were pre-treated with NAC (10 mM) for 1 h.

3.8. Induction of mitochondrial dysfunction

As demonstrated in the literature, once the intact mitochondrial membrane is disrupted, the pro-apoptotic factors are released from mitochondria and initiate the apoptotic pathway cascade [45]. In order to investigate whether alteration of mitochondrial membrane potential (ΔΨm) was involved in induction of cell death, the ΔΨm in A549 cancer cells was stained with a fluorescent probe JC-1, followed by detecting with flow cytometry. As shown in Fig. 5, Fig. S15 and Table S6, ESI†, implying that Ir2 treatment for 24 h significantly depolarized ΔΨm in a concentration-dependent manner.

3.9. Induction of cellular ROS

Effects of ROS on numerous biological and physiological responses are well recognised in many species. Examples of these cellular

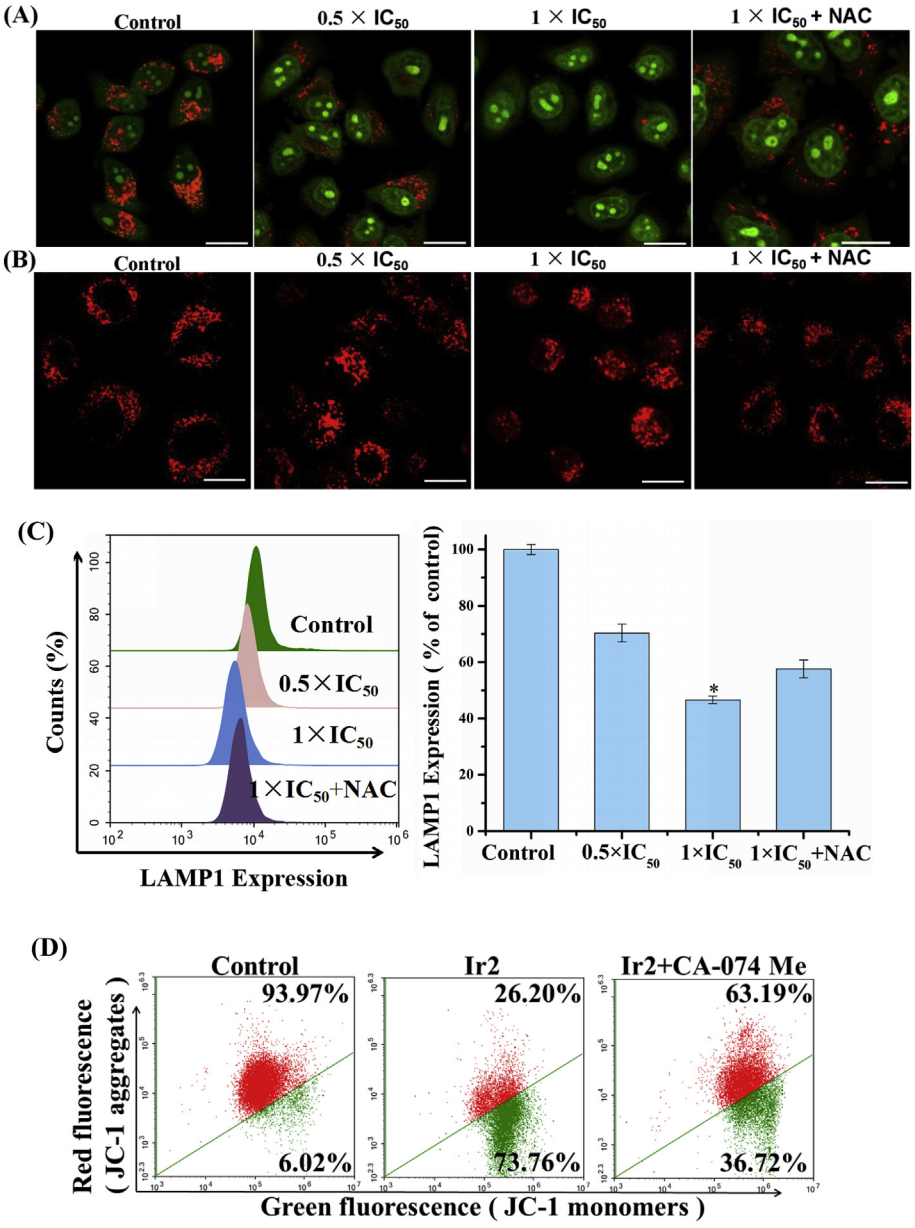

Fig. 7. NAC decreased lysosomal disruption in Ir2-treated cells. A549 cells were treated with Ir2 by indicated concentrations for 24 h in the absence or presence of NAC (10 mM) pretreatment for 1 h followed by (A) staining with AO (5 μM) staining. λ_{ex} = 488 nm, λ_{em} = 520 ± 20 nm (green) and 630 ± 20 nm (red). Scale bars: 20 μm. (B) Observation of cathepsin B release from lysosomes to the cytosol with Magic Red MR-$(RR)_2$ staining. λ_{ex} = 594 nm λ_{em} = 620 ± 20 nm. Scale bars: 20 μm. (C) Levels of LAMP1 expression were measured using flow cytometry (*P < 0.01 vs Control). (D) Changes in mitochondrial membrane potential of A549 cancer cells induced by Ir2 at 1 × IC_{50} for 24 h in the absence or presence of CA-074 Me (5 mM) pretreatment for 2 h followed by staining with JC-1 and measured using flow cytometry. (For interpretation of the references to colour in this figure legend, the reader is referred to the Web version of this article.)

processes include the role in cell proliferation and apoptosis [46]. Therefore, we tested the intracellular ROS status in A549 cells induced by Ir2 using flow cytometry analysis. Treatment of A549 cells with Ir2 and ROS levels were measured after staining with 2′,7′-dichlorofluorescein diacetate (DCFH-DA). It was observed that Ir2 increased significantly even at 0.5 × IC_{50} concentration the ROS levels by 4-fold in A549 cells after treatment for 24 h compared to the ROS levels of control cells. Moreover, pretreatment with the N-acetylcysteine (NAC), a direct scavenger of ROS, evidently diminished the Ir-elevated generation of ROS in A549 cells (Fig. 6 and Table S7, ESI†). These data suggest that ROS could be involved in the Ir2-induced cytotoxicity.

3.10. Effects of NAC and CA-074 Me on the lysosomal disruption and mitochondrial dysfunction in Ir2-treated cells, respectively

Emerging evidence supports that the notion ROS has been shown to cause lysosomal disruption by the peroxidation of membrane lipids [47]. In order to explore the role of ROS in regulating the mitochondria-lysosome cross-talk, firstly, we investigated the effect of Ir2 on lysosomal stability, a fluorescent probe of lysosome, acridine orange (AO), was used to study the integrity of the lysosome. AO staining appears as green fluorescence in nuclei and cytosol, but red fluorescence in lysosomes. A549 cells were treated with Ir2 with or without ROS scavenger NAC for 24 h and followed by confocal microscopy analysis. The red fluorescence visibly decreased when the A549 cells were treated with Ir2 (1 × IC_{50}). Additionally, the red fluorescence in A549 cells that received Ir2 (1 × IC_{50}) and NAC pretreatment was remarkably raised in comparison with the A549 cells that received the Ir2 (1 × IC_{50}) treatment alone (Fig. 7A), which implied that NAC protected A549 cells from Ir2-induced lysosome disruption. Lysosome disruption could cause the release of lysosomal hydrolases, particularly cathepsin B, into the cytosol to promote apoptosis [48]. To assess whether overproduction of ROS was involved in Ir2-induced cathepsin B release, A549 cells were treated with Ir2 in the presence or absence of NAC. The fluorogenic cathepsin B substrate Magic Red MR-$(RR)_2$ was used for detecting the activity of cathepsin B. The red fluorescence mainly localized in the lysosomes in A549 cell control group, while Ir2 (1 × IC_{50})-treated A549 cells mostly showed a diffused red fluorescence. Additionally, the diffused red fluorescence in A549 cells that received Ir2 (1 × IC_{50}) and NAC pretreatment was rescued compared with the A549 cells that

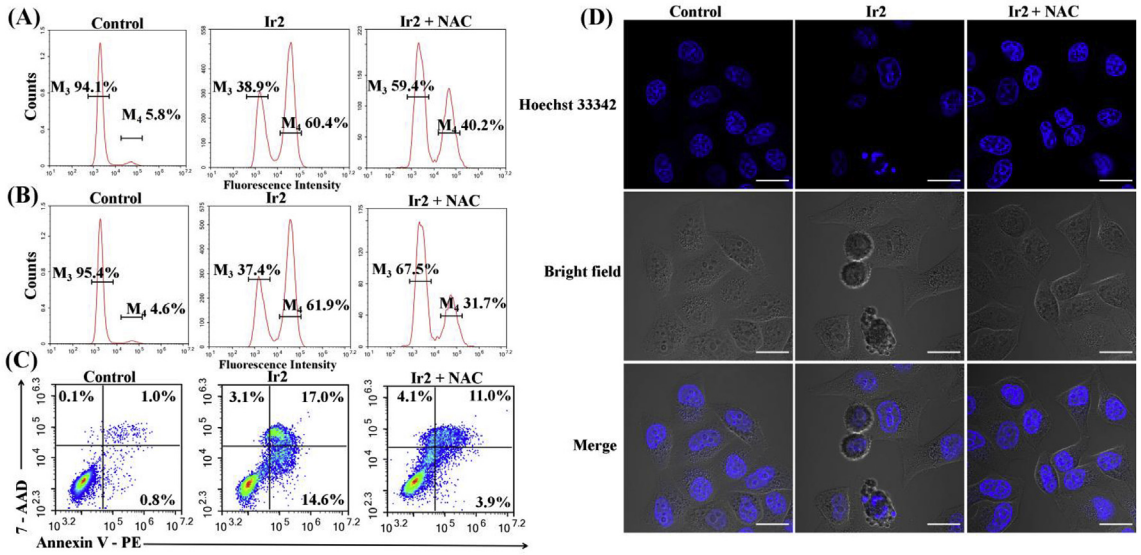

Fig. 8. ROS plays a key role in Ir2 complex-induced apoptosis in A549 cells. NAC (10 mM) pre-treatment reduced the expression of cleaved caspase 3 (A) and cleaved PARP (B) and percentage of apoptosis (C、D) in Ir2 (1 × IC_{50}) - treated A549 cells for 24 h.

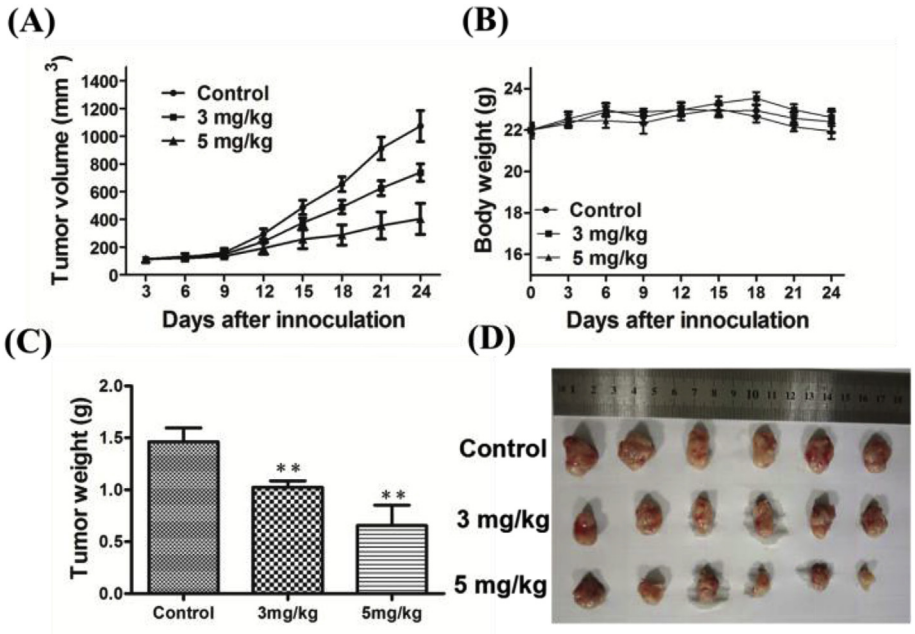

Fig. 9. (A) Average tumor volumes of mice CT26 xenograft-bearing mice treated with vehicle or Ir2 through intravenous injection at 3 mg/kg and 5 mg/kg daily for 7 days (n = 6). (B) Body weight of mice in different treatment groups. (C) Average tumors weight of mice at the end of the experiment in different treatment groups (**P < 0.01 vs Control). (D) Tumors separated from CT26 xenograft-bearing mice.

received the Ir2 (1 × IC_{50}) treatment alone (Fig. 7B), which indicated that NAC protected A549 cells from Ir2-induced cathepsin B release from lysosome to cytosol. ROS-induced down-regulation of Lysosome-associated membrane proteins (LAMPs) expression could lead to lysosomal disruption [49]. To investigate whether overproduction of ROS is involved in the Ir2-induced down-regulation of LAMP1 expression, A549 cells were treated with Ir2 with or without NAC for 24 h. The results indicated that LAMP1 protein levels significantly decreased with the Ir2 treatment and with a partial restoration of LAMP1 levels observed with NAC pretreatment (Fig. 7C). Finally, to ascertain the role of cathepsin B in Ir-induced mitochondrial dysfunction, A549 cells were pretreated with CA-074 Me, a cell-permeable-specific cathepsin B inhibitor, at a dose of 5 mM for 2 h. The results suggested that CA-074 Me partially reduced mitochondrial dysfunction from Ir2-treated cells (Fig. 7D, Fig. S16 and Table S8, ESI†). Together, these results showed that Ir2 induced lysosome disruption by decreasing LAMP1 expression, following the increase in cathepsin B leakage into the cytoplasm in A549 cells, NAC protected A549 cells from Ir2-induced lysosome damage, and that the cross-talk between mitochondria and lysosomes was mediated by ROS.

3.11. ROS plays a key role in Ir2-mediated cell apoptosis

Since Ir2 exhibited potent apoptosis induction and ROS overproduction in A549 cells as discussed above, we further investigated whether ROS has any role in Ir2 induced cell apoptosis. A549 cells were treated for 24 h with Ir2 with or without ROS scavenger NAC pretreatment for 2 h and followed by flow cytometry and confocal microscopy analysis. NAC pre-treatment clearly decreased the Ir2-induced expression of cleaved caspase 3 and stimulated proteolytic cleavage of poly ADP-ribose polymerase (PARP), which is susceptible to caspase 3, as summarized in Fig. 8A and B, Fig. S17, S18 and Tables S9, S10, ESI†. Meanwhile, NAC pre-treatment also reduced the Ir2-induced percentage of apoptosis (Fig. 8C). Moreover, pro-apoptotic protein Bax was

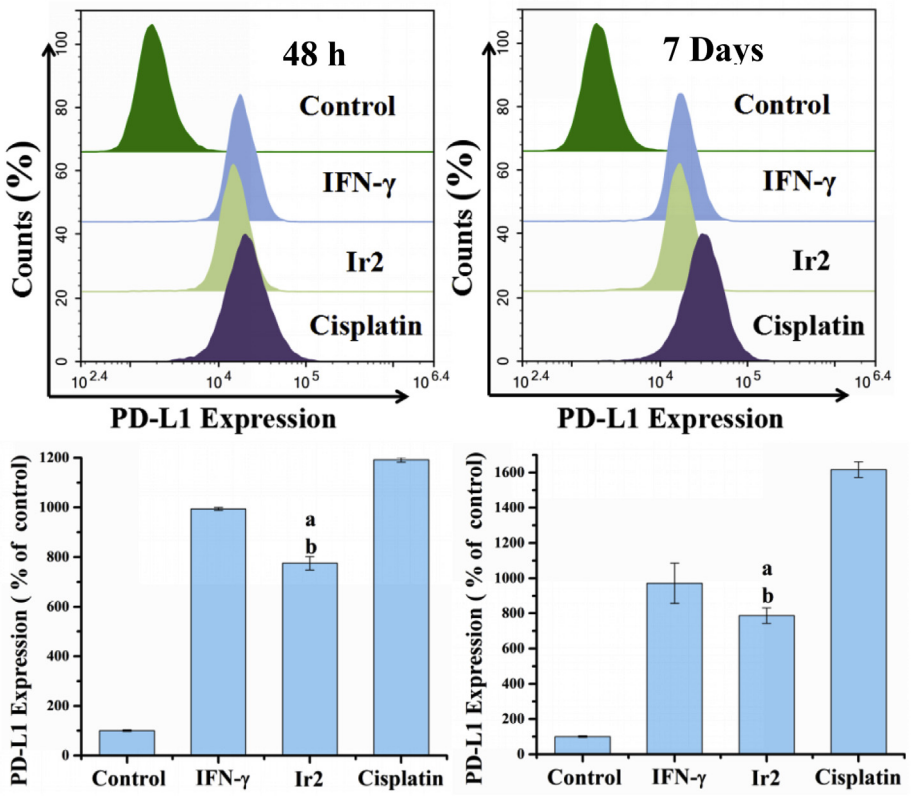

Fig. 10. The PD-L1 expression in complex Ir2 (0.5 × IC_{50}), cisplatin (0.5 × IC_{50}) and IFN-γ (20 ng/ml)-treated A549 cells for 48 h and 7 days. Levels of PD-L1 expression were determined by flow cytometry ($^{a}P < 0.05$ vs Control, $^{b}P < 0.05$ vs Cisplatin).

Table 2
Combination index (CI) value of cisplatin with Ir2 (μM) against A549 cancer cells.

	Cisplatin	Ir2	CI at IC_{50}
Cisplatin	21.30 ± 1.72	–	
Ir2	–	3.70 ± 0.53	
Cisplatin: Ir2 = 1:1	2.81 ± 0.68	2.81 ± 0.68	0.88 ± 0.07

upregulated and the antiapoptotic protein Bcl-2 was downregulated in A549 cells after treatment with Ir2; however, NAC reduced Ir2-induced the expression level of Bax,simultaneously, and increased Ir2-induced the expression level of Bcl-2 (Fig. S19). In addition, changes in cell morphology upon Ir2-mediated apoptosis were further examined by Hoechst 33342 staining assay. Ir2 treatment caused apoptosis characterized by nuclear condensation, cell shrinkage, and membrane blebbing observed by confocal microscopy, while these apoptotic features could be counteracted by NAC (Fig. 8D). These findings show that the ROS overproduction is a crucial event in Ir2-induced apoptosis.

3.12. Inhibition of tumor growth in mice xenograft model

In vivo the anti-tumor effect of Ir2 was assessed in a CT26 colon cancer mouse xenograft model. On day 3 after tumor inoculation, control group mice received the vehicle (2.5% DMSO and 97.5% of a saline solution (v/v)), whereas treatment groups received doses of Ir2 (3 mg/kg and 5 mg/kg dissolved in a vehicle solution) daily for 7 days. On day 24, mice were sacrificed and tumor growth was determined. As shown in Fig. 9A, the rate of tumor growth was inhibited by up to 31.2% (3 mg/kg) and 62.3% (5 mg/kg), respectively, as compared to a vehicle control. In parallel, Ir2 reduced the tumor weight by 31.8% (3 mg/kg) ($P < 0.01$) and 56.4% (5 mg/kg) ($P < 0.01$) compared to control, respectively (Fig. 9C and D). Importantly, outward signs of Ir2 (3 mg/kg and 5 mg/kg) toxicity and obvious body weight loss were not observed during the experiment (Fig. 9B), suggesting that Ir2 was well tolerated *in vivo*.

3.13. Induction of PD-L1 expression

Recently, clinical studies have suggested that expression of programmed death ligand 1 (PD-L1) is involved in chemotherapy resistance, and upregulation of PD-L1 expression after chemotherapy has been identified as a marker of poor prognosis in patients with cancers [50]. To validate the effects of Ir complexes on PD-L1 expression status, A549 cells were treated with Ir2, cisplatin and IFN-γ (positive control) for 48 h and 7 days, followed by flow cytometry analysis. A549 cells treated with Ir2 (0.5 × IC_{50}), cisplatin (0.5 × IC_{50}) and IFN-γ (20 ng/ml) for 48 h led to an increase in expression of PD-L1. However, compared with the Ir2 group, higher levels of PD-L1 expression were observed in A549 cells after treatment with cisplatin for 48 h. To further measure the effects of chronic exposure to low concentrations of complex Ir2 (0.25 × IC_{50}), cisplatin (0.25 × IC_{50}) and IFN-γ (20 ng/ml) on PD-L1 expression status, after incubation of A549 cells for 7 days, levels of PD-L1 expression were ~2 fold higher in the cisplatin group compared to the Ir2 group (Fig. 10). These data suggest that Ir2 could provoke less immunosuppression and induction of chemotherapy resistance involved in PD-L1 expression compared with cisplatin *in vitro*. Next we investigated whether Ir2 could enhance the cytotoxicity of cisplatin in A549 cells. Table 2 indicated that the combination of cisplatin and Ir2 exerted slight synergistic cytotoxic activity with the combination index (CI) of 0.88 ($CI < 1$) at IC_{50} against A549 cells (Table 2). Notably, PD-L1 expression was slightly downregulated by cisplatin and Ir2 combination treatment, compared with cisplatin or Ir2 alone (Fig. S20). These results suggested that combination of Ir2 and cisplatin could regulate cisplatin resistance through PD-L1.

In conclusion, we have synthesized and characterized four half-

sandwich Ir^{III} complexes [(η^5-Cp^{xbiph})Ir(O^C)Cl]. These Ir^{III} complexes exert more potent antiproliferative activity compared to cisplatin against 7 cancer cell lines. Complex Ir2 is 8-fold more potent than cisplatin. Ir2 can effectively impede critical cancerous processes, further MoA studies indicate that ROS exerts a key role in Ir2-triggered apoptosis and may act as a messenger between mitochondria and lysosome. In addition, Ir2 can also dramatically curb tumor growth *in vivo*. Finally, Ir2 could provoke less induction of chemotherapy resistance compared with cisplatin. Therefore the present study sheds new light on half-sandwich Ir^{III} complexes with their combined features of antimetastasis and anticancer activity *in vitro* and *in vivo* that warrant further development.

Conflicts of interest

There are no conflicts of interest to declare.

Acknowledgements

This work was supported by National Science Foundation of China (Grant No. 21671118) and the Taishan Scholars Program.

Appendix A. Supplementary data

Supplementary data to this article can be found online at https://doi.org/10.1016/j.canlet.2019.01.018.

References

[1] H.J. Burstein, L. Krilov, J.B. Aragon-Ching, N.N. Baxter, E.G. Chiorean, W.A. Chow, et al., Clinical Cancer Advances 2017: annual report on progress against cancer from the american society of clinical oncology, J. Clin. Oncol. 35 (2017) 1341–1367.
[2] P. Friedl, S. Alexander, Cancer invasion and the microenvironment: plasticity and reciprocity, Cell 147 (2011) 992–1009.
[3] M. Nikolaou, A. Pavlopoulou, A.G. Georgakilas, E. Kyrodimos, The challenge of drug resistance in cancer treatment: a current overview, Clin. Exp. Metastasis 35 (2018) 309–318.
[4] V. Adorno-Cruz, G. Kibria, X. Liu, M. Doherty, D.J. Junk, D. Guan, et al., Cancer stem cells: targeting the roots of cancer, seeds of metastasis, and sources of therapy resistance, Cancer Res. 75 (2015) 924–929.
[5] S. Dasari, P.B. Tchounwou, Cisplatin in cancer therapy: molecular mechanisms of action, Eur. J. Pharmacol. 740 (2014) 364–378.
[6] A.M. Florea, D. Busselberg, Cisplatin as an anti-tumor drug: cellular mechanisms of activity, drug resistance and induced side effects, Cancers 3 (2011) 1351–1371.
[7] R. Trondl, P. Heffeter, C.R. Kowol, M.A. Jakupec, W. Berger, B.K. Keppler, NKP-1339, the first ruthenium-based anticancer drug on the edge to clinical application, Chem. Sci. 5 (2014) 2925–2932.
[8] K. Arora, M. Herroon, M.H. Al-Afyouni, N.P. Toupin, T.N. Rohrabaugh Jr., L.M. Loftus, et al., Catch and release photosensitizers: combining dual-action ruthenium complexes with protease inactivation for targeting invasive cancers, J. Am. Chem. Soc. 140 (2018) 14367–14380.
[9] C.S. Burke, A. Byrne, T.E. Keyes, Targeting photoinduced DNA destruction by ru(II) tetraazaphenanthrene in live cells by signal peptide, J. Am. Chem. Soc. 140 (2018) 6945–6955.
[10] J. Li, L. Guo, Z. Tian, S. Zhang, Z. Xu, Y. Han, et al., Half-sandwich iridium and ruthenium complexes: effective tracking in cells and anticancer studies, Inorg. Chem. 57 (2018) 13552–13563.
[11] J. Li, Z. Tian, Z. Xu, S. Zhang, Y. Feng, L. Zhang, et al., Highly potent half-sandwich iridium and ruthenium complexes as lysosome-targeted imaging and anticancer agents, Dalton Trans. 47 (2018) 15772–15782.
[12] W. Ma, X. Ge, L. Guo, S. Zhang, J. Li, X. He, et al., Bichromophoric anticancer drug: targeting lysosome with rhodamine modified cyclometalated iridium(III) complexes, Dyes Pigments 162 (2019) 385–393.
[13] Z. Liu, A. Habtemariam, A.M. Pizarro, S.A. Fletcher, A. Kisova, O. Vrana, et al., Organometallic half-sandwich iridium anticancer complexes, J. Med. Chem. 54 (2011) 3011–3026.
[14] Z. Liu, I. Romero-Canelon, B. Qamar, J.M. Hearn, A. Habtemariam, N.P. Barry, et al., The potent oxidant anticancer activity of organoiridium catalysts, Angew. Chem. Int. Ed. 53 (2014) 3941–3946.
[15] L. He, C.-P. Tan, R.-R. Ye, Y.-Z. Zhao, Y.-H. Liu, Q. Zhao, et al., Theranostic iridium (III) complexes as one- and two-photon phosphorescent trackers to monitor autophagic lysosomes, Angew. Chem. Int. Ed. 53 (2014) 12137–12141.
[16] M. Ouyang, L. Zeng, H. Huang, C. Jin, J. Liu, Y. Chen, et al., Fluorinated cyclometalated iridium(iii) complexes as mitochondria-targeted theranostic anticancer agents, Dalton Trans. 46 (2017) 6734–6744.
[17] L.J. Liu, W. Wang, S.Y. Huang, Y. Hong, G. Li, S. Lin, et al., Inhibition of the Ras/Raf interaction and repression of renal cancer xenografts in vivo by an enantiomeric iridium(iii) metal-based compound, Chem. Sci. 8 (2017) 4756–4763.
[18] T.S. Kang, W. Wang, H.J. Zhong, Z.Z. Dong, Q. Huang, S.W. Mok, et al., An anti-prostate cancer benzofuran-conjugated iridium(III) complex as a dual inhibitor of STAT3 and NF-kappaB, Cancer Lett. 396 (2017) 76–84.
[19] J.M. Hearn, I. Romero-Canelon, B. Qamar, Z. Liu, I. Hands-Portman, P.J. Sadler, Organometallic Iridium(III) anticancer complexes with new mechanisms of action: NCI-60 screening, mitochondrial targeting, and apoptosis, ACS Chem. Biol. 8 (2013) 1335–1343.
[20] Z. Liu, I. Romero-Canelon, A. Habtemariam, G.J. Clarkson, P.J. Sadler, Potent Half-sandwich iridium(III) anticancer complexes containing C(wedge)N-chelated and pyridine ligands, Organometallics 33 (2014) 5324–5333.
[21] D.L. Ma, C. Wu, W. Tang, A.-R. Gupta, F.-W. Lee, G. Li, C.-H. Leung, Recent advances in iridium(iii) complex-assisted nanomaterials for biological applications, J. Mater. Chem. B 6 (2018) 537–544.
[22] D.L. Ma, S. Lin, W. Wang, C. Yang, C.H. Leung, Luminescent chemosensors by using cyclometalated iridium(iii) complexes and their applications, Chem. Sci. 8 (2017) 878–889.
[23] M. Tian, J. Li, S. Zhang, L. Guo, X. He, D. Kong, et al., Half-sandwich ruthenium(ii) complexes containing N^N-chelated imino-pyridyl ligands that are selectively toxic to cancer cells, Chem. Commun. 53 (2017) 12810–12813.
[24] J. Li, M. Tian, Z. Tian, S. Zhang, C. Yan, C. Shao, et al., Half-sandwich iridium(III) and ruthenium(II) complexes containing P^P-chelating ligands: a new class of potent anticancer agents with unusual redox features, Inorg. Chem. 57 (2018) 1705–1716.
[25] H. Zhang, L. Guo, Z. Tian, M. Tian, S. Zhang, Z. Xu, et al., Significant effects of counteranions on the anticancer activity of iridium(iii) complexes, Chem. Commun. 54 (2018) 4421–4424.
[26] Z. Tian, J. Li, S. Zhang, Y. Yang, Z. Xu, D. Kong, et al., Lysosome-targeted chemotherapeutics: half-sandwich ruthenium(II) complexes that are selectively toxic to cancer cells, Inorg. Chem. 57 (2018) 10498–10502.
[27] W. Ma, Z. Tian, S. Zhang, X. He, J. Li, X. Xia, et al., Lysosomal Targeted Drugs: rhodamine B modified N^N-chelating ligands for half-Sandwich Iridium(III) anticancer complexes, Inorg. Chem. Front. 5 (2018) 2587–2597.
[28] Z. Xu, D. Kong, X. He, L. Guo, X. Ge, H. Zhang, et al., Mitochondria-targeted half-sandwich rutheniumII diimine complexes: anticancer and antimetastasis via ROS-mediated signalling, Inorg. Chem. Front. 5 (2018) 2100–2105.
[29] Y. Yang, L. Guo, Z. Tian, Y. Gong, H. Zheng, S. Zhang, Novel and versatile imine-N-heterocyclic carbene half-sandwich iridium(III) complexes as lysosome-targeted anticancer agents, Inorg. Chem. 57 (2018) 11087–11098.
[30] F. Cisnetti, A. Gautier, Metal/N-heterocyclic carbene complexes: opportunities for the development of anticancer metallo drugs, Angew. Chem. Int. Ed. 52 (2013) 11976–11978.
[31] T.T. Fong, C.N. Lok, C.Y. Chung, Y.M. Fung, P.K. Chow, P.K. Wan, et al., Cyclometalated palladium(II) N-heterocyclic carbene complexes: anticancer agents for potent in vitro cytotoxicity and in vivo tumor growth suppression, Angew. Chem. Int. Ed. 55 (2016) 11935–11939.
[32] D. Yang, Y. Tang, H. Song, B. Wang, o-Aryloxide-N-heterocyclic carbenes: efficient synthesis of the proligands and their p-cymene ruthenium complexes, Organometallics 34 (2015) 2012–2017.
[33] K.Y. Wan, M.M.H. Sung, A.J. Lough, R.H. Morris, Half-sandwich suthenium catalyst bearing an enantiopure primary amine tethered to an N-heterocyclic carbene for ketone hydrogenation, ACS Catal. 7 (2017) 6827–6842.
[34] Y. Li, C.-P. Tan, W. Zhang, L. He, L.-N. Ji, Z.-W. Mao, Phosphorescent iridium(III)-bis-N-heterocyclic carbene complexes as mitochondria-targeted theranostic and photodynamic anticancer agents, Biomaterials 39 (2015) 95–104.
[35] K.i. Fujita, R. Tamura, Y. Tanaka, M. Yoshida, M. Onoda, R. Yamaguchi, Dehydrogenative oxidation of alcohols in aqueous media catalyzed by a water-soluble dicationic iridium complex bearing a functional N-heterocyclic carbene ligand without using base, ACS Catal. 7 (2017) 7226–7230.
[36] C. Wang, J. Liu, Z. Tian, M. Tian, L. Tian, W. Zhao, et al., Half-sandwich iridium N-heterocyclic carbene anticancer complexes, Dalton Trans. 46 (2017) 6870–6883.
[37] S. Zhang, X. Li, H. Sun, O. Fuhr, D. Fenske, Nickel(II) complexes of amine functionalized N-heterocyclic carbenes (NHCs), synthesis and catalysis in Kumada coupling of aryl chlorides, J. Organomet. Chem. 820 (2016) 41–45.
[38] D. Gülcemal, S. Gülcemal, C.M. Robertson, J. Xiao, A new phenoxide chelated IrIII N-heterocyclic carbene complex and its application in reductive amination reactions, Organometallics 34 (2015) 4394–4400.
[39] Z. Zhao, Z. Luo, Q. Wu, W. Zheng, Y. Feng, T. Chen, Mixed-ligand ruthenium polypyridyl complexes as apoptosis inducers in cancer cells, the cellular translocation and the important role of ROS-mediated signaling, Dalton Trans. 43 (2014) 17017–17028.
[40] Y. Zheng, L. He, D.Y. Zhang, C.P. Tan, L.N. Ji, Z.W. Mao, Mixed-ligand iridium(iii) complexes as photodynamic anticancer agents, Dalton Trans. 46 (2017) 11395–11407.
[41] G.P. Gupta, J. Massague, Cancer metastasis: building a framework, Cell 127 (2006) 679–695.
[42] K. Vellaisamy, G. Li, W. Wang, C.-H. Leung, D.-L. Ma, A long-lived peptide-conjugated iridium(iii) complex as a luminescent probe and inhibitor of the cell migration mediator, formyl peptide receptor 2, Chem. Sci. 9 (2018) 8171–8177.
[43] S. Valastyan, R.A. Weinberg, Tumor metastasis: molecular insights and evolving paradigms, Cell 147 (2011) 275–292.
[44] X. He, M. Tian, X. Liu, Y. Tang, C.F. Shao, P. Gong, et al., Triphenylamine-appended half-sandwich iridium(III) complexes and their biological applications, Chem. Asian J. 13 (2018) 1500–1509.
[45] J. Liu, Y. Chen, G. Li, P. Zhang, C. Jin, L. Zeng, et al., Ruthenium(II) polypyridyl complexes as mitochondria-targeted two-photon photodynamic anticancer agents,

Biomaterials 56 (2015) 140–153.
[46] L.A. Sena, N.S. Chandel, Physiological roles of mitochondrial reactive oxygen species, Mol. Cell. 48 (2012) 158–167.
[47] P. Boya, G. Kroemer, Lysosomal membrane permeabilization in cell death, Oncogene 27 (2008) 6434–6451.
[48] M.E. Heid, P.A. Keyel, C. Kamga, S. Shiva, S.C. Watkins, R.D. Salter, Mitochondrial reactive oxygen species induces NLRP3-dependent lysosomal damage and inflammasome activation, J. Immunol. 191 (2013) 5230–5238.
[49] X. Yan, T. Ye, X. Hu, P. Zhao, X. Wang, 58-F, a flavanone from Ophiopogon japonicus, prevents hepatocyte death by decreasing lysosomal membrane permeability, Sci. Rep. 6 (2016) 27875.
[50] W. Gong, Q. Song, X. Lu, W. Gong, J. Zhao, P. Min, X. Yi, Paclitaxel induced b7-H1 expression in Cancer Cells via the MApK pathway, J. Chemother. 23 (2011) 295–299.